JOURNAL OF APPLIED PHYSICS **119**, 085104 (2016)

Localized Mg-vacancy states in the thermoelectric material $Mg_{2-\delta}Si_{0.4}Sn_{0.6}$

Libin Zhang,[1,a)] Penghao Xiao,[2] Li Shi,[1,3] Graeme Henkelman,[2] John B. Goodenough,[1,3] and Jianshi Zhou[1,3]

[1]*Materials Science and Engineering Program, University of Texas at Austin, Austin, Texas 78712, USA*
[2]*Department of Chemistry and the Institute for Computational and Engineering Sciences, University of Texas at Austin, Austin, Texas 78712, USA*
[3]*Department of Mechanical Engineering, The University of Texas at Austin, Austin, Texas 78712, USA*

(Received 5 October 2015; accepted 3 February 2016; published online 25 February 2016)

$Mg_2Si_xSn_{1-x}$ has been widely studied as a thermoelectric material owing to its high figure-of-merit, low cost, and non-toxicity. However, its electronic structure, particularly when the material contains Mg vacancies, has not been adequately described. The n-type nature of $Mg_{2-\delta}Si_{0.4}Sn_{0.6}$ has been a puzzle. Mg deficiency can be present in $Mg_2Si_xSn_{1-x}$ due to Mg evaporation and oxidation. Therefore, an investigation of the role of Mg vacancies is of great interest. In this work, we have prepared a series of samples with various Mg deficiency and Sb doping levels and measured their transport properties. The Seebeck coefficient of these samples all reveals n-type conduction. We propose that Mg vacancies in $Mg_{2-\delta}Si_xSn_{1-x}$ create localized hole states inside the band gap instead of simply moving the Fermi-level into the valence band as would be predicted by a rigid band model. Our hypothesis is further confirmed by density-functional theory calculations, which show that the hole states are trapped at Mg vacancies above the valence band. Moreover, this localized hole-states model is used to interpret electrical transport properties. Both the Seebeck coefficient and resistivity of $Mg_{2-\delta}Si_{0.4}Sn_{0.6}$ indicate an electron-hopping transport mechanism. In addition, the data suggest that localized band-tail states may exist in the conduction-band edge of $Mg_2Si_xSn_{1-x}$. © *2016 AIP Publishing LLC*. [http://dx.doi.org/10.1063/1.4942012]

I. INTRODUCTION

Thermoelectric (TE) materials have attracted increasing research interests due to their applications in waste heat recovery and refrigeration. $Mg_2Si_xSn_{1-x}$ is one of the high performance, state-of-the-art n-type thermoelectric materials. $Mg_2Si_xSn_{1-x}$ has an anti-fluorite crystal structure with the space group $Fm\bar{3}m$. Intrinsic $Mg_2Si_xSn_{1-x}$ is a semiconductor with a band gap between 0.3 and 0.7 eV depending on the Si/Sn ratio. With an optimized concentration of Sb (or Bi) doping, $Mg_2Si_xSn_{1-x}$ exhibits a desirable metallic conductivity (σ) while maintaining a high magnitude of Seebeck coefficient (S). Given a relatively low thermal conductivity (κ) due to the alloying effect, $Mg_2Si_xSn_{1-x}$ can achieve a desirable figure of merit ($ZT = \frac{S^2\sigma}{\kappa}T$) of 1.0 to 1.4 at 750 K.[1–3]

During the synthesis and consolidation processes of $Mg_2Si_xSn_{1-x}$, a significant amount of Mg is lost due to Mg vaporization and oxidation to MgO. The material becomes Mg-deficient if the stoichiometric ratio of components is used in the synthesis. Practically then, excess Mg is added when synthesizing the material to compensate for the Mg loss. It is still possible, however, that Mg vacancies may form during the synthesis and subsequent heat treatments. Nolas *et al*. pointed out that Mg vacancies could behave as electron acceptors and counteract the contribution of electron dopants.[4–6] Tobola *et al*. believed that in intrinsic $Mg_{2-\delta}Si$, Mg vacancies act as double-hole donors that would shift the Fermi level into the valence band and give rise to a p-type Seebeck coefficient.[7] To the best of our knowledge, however, a p-type Seebeck coefficient has not been reported in an undoped Mg_2Si, Mg_2Sn, or $Mg_2Si_xSn_{1-x}$ solid solution, even though it is possible to introduce Mg vacancies unintentionally during synthesis. This discrepancy motivates us to investigate the influence of Mg vacancies on the band structures and transport properties of $Mg_2Si_xSn_{1-x}$.

In this work, we prepared Mg-deficient $Mg_2Si_{0.4}Sn_{0.6}$ samples and observed intriguing physical properties. Two observations contradict the predictions from a rigid-band model. First of all, intrinsic $Mg_{2-\delta}Si_{0.4}Sn_{0.6}$ containing Mg vacancies exhibits n-type conduction as indicated by Seebeck and Hall-coefficient measurements. Second, the electron concentration does not increase in the 1.5 mol. % Sb doped $Mg_{2-\delta}Si_{0.4}Sn_{0.6}$ relative to that of the intrinsic sample. We suggest that Mg vacancies in these samples create localized hole states instead of contributing free holes. In order to verify this hypothesis, we investigated the electronic structures using density functional theory (DFT) calculations. The calculations indeed show that Mg vacancies create localized states within the band gap, while the Fermi level lies in between the valence band and the Mg-vacancy states. This localized-state picture explains the peculiar transport properties of intrinsic and Sb-doped $Mg_{2-\delta}Si_{0.4}Sn_{0.6}$. In addition, we also found that Anderson localized states are likely to present at the conduction band tail, which induces a metal-insulator-transition (MIT) in the lightly n-doped $Mg_2Si_{0.4}Sn_{0.6}$.

II. METHODS

The $Mg_2Si_{0.4}Sn_{0.6}$ samples were prepared by a one-step solid-state reaction followed by spark plasma sintering

a)libinzhang@utexas.edu

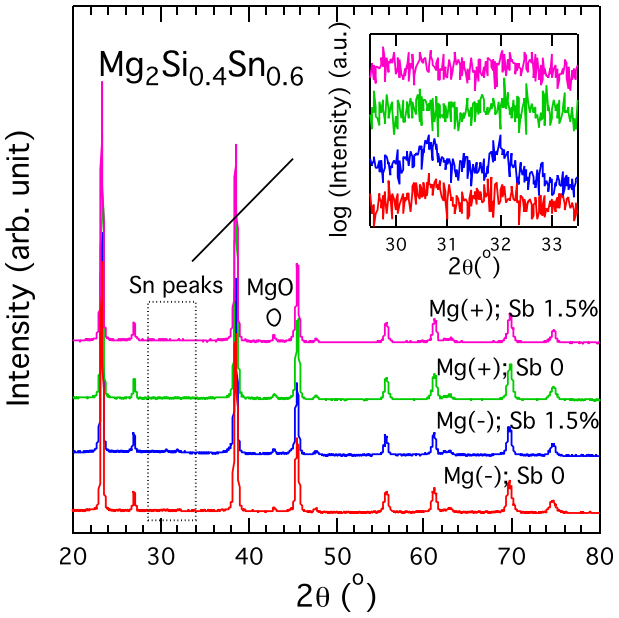

FIG. 1. X-ray diffraction patterns of four different $Mg_2Si_{0.4}Sn_{0.6}$ samples. The inset shows that peaks at 30°–33° from Sn appear in the two Mg(–) samples (red and blue curves), but not in the two Mg(+) samples (green and pink curves).

(SPS). The detailed procedure can be found in Ref. 8. The crystal structure of the samples was characterized by X-ray diffraction (XRD) on a Rigaku MiniFlex 600 with the Cu Kα radiation. The Hall coefficients from 2 K to 400 K were measured with a Physical Properties Measurement System (PPMS, Quantum Design) by using a 4-wire method. The Seebeck coefficient and electrical conductivity were also measured from 2 K to 400 K simultaneously with the PPMS by using its thermal transport option.

The electronic structures were calculated by using density functional theory. The projector augmented wave method was used to describe the core electrons and a plane wave basis set, with an energy cutoff of 246 eV, was used to describe the valence electrons.[9,10] The structures were optimized at the Perdew-Burke-Ernzerhof (PBE) level of theory,[11] while the density of states (DOS) was calculated with the hybrid Heyd-Scuseria-Ernzerhof functional.[12–14]

III. RESULTS AND ANALYSIS

Based on many trial-and-error experiments, we have determined that over 14 to 16 mol. % of excess Mg should be compensated in the starting materials in order to prepare stoichiometric $Mg_2Si_{0.4}Sn_{0.6}$ solid solutions, since a significant amount of Mg is lost during the synthesis and consolidation procedure described in Ref. 8. To prepare slightly Mg-deficient $Mg_2Si_{0.4}Sn_{0.6}$ samples, we compensate only with 12 mol. % excess Mg in the starting materials. For comparison, we also prepared the Mg-stoichiometric samples by adding 17 mol. % excess Mg in the starting material. To simplify the notation, we denote the $Mg_2Si_{0.4}Sn_{0.6}$ samples with 12 mol. % of excess Mg in the starting material as the Mg(–) samples and those with 17 mol. % of excess Mg as the Mg(+) samples. The subscript $_{in}$ or $_{Sb}$ is used to denote the intrinsic or Sb-doped sample. For example, $Mg(-)_{in}$ stands for the intrinsic $Mg_2Si_{0.4}Sn_{0.6}$ compensated with 12 mol. % excess Mg, while $Mg(+)_{Sb}$ stands for the 1.5 mol. % Sb-doped $Mg_2Si_{0.4}Sn_{0.6}$ compensated with 17 mol. % excess Mg in the starting materials.

A. Material characterizations

In Fig. 1 and its inset, the XRD patterns of the Mg(–) samples (red and blue curves) show two small peaks around 30°–33°, which are due to a Sn impurity phase. These two peaks are absent in the Mg(+) samples (green and pink). The precipitation of Sn phase indicates that 12% extra Mg cannot fully compensate for the Mg loss during the sample preparation. However, it is unknown whether Mg vacancies exist in the major $Mg_2Si_{0.4}Sn_{0.6}$ phase even though Mg is deficient. To look for the presence of Mg vacancy in the lattice of Mg(–) samples, we performed a Rietveld refinement of the XRD data to determine the Mg site occupancy ($Occ._{Mg}$). Since the occupancy is highly correlated with the thermal parameters B_{iso}, we fixed the B_{iso} at an optimized value for all the refinements. As shown in Table I, $Occ._{Mg}$ in both Mg(+) samples are close to the stoichiometric value of 2. On the other hand, $Occ._{Mg}$ are 1.986 and 1.972 for $Mg(-)_{in}$ and $Mg(-)_{Sb}$, respectively, indicating that a small fraction of Mg vacancies (1.4 to 2.8 mol. %) exists in the Mg(–) samples. In addition, Sb doping appears to lower the $Occ._{Mg}$ of $Mg(-)_{Sb}$ relative to that of $Mg(-)_{in}$, in agreement with the observations made in the previous studies.[4–6] The lattice parameters of the Mg(–) samples are slightly smaller than those of their Mg(+) counterparts, possibly due to the precipitation of Sn element. However, the change of lattice parameters is so small that the change of the Si/Sn ratio is not important for our results.

B. Transport properties

The temperature-dependent transport properties of all $Mg_2Si_{0.4}Sn_{0.6}$ samples are shown in Fig. 2. For the Mg(+) samples, 1.5 mol. % Sb doping effectively induces a change in the material from a non-degenerate semiconductor to a degenerate one. As shown in Fig. 2(a), the electron concentration (n_H) of $Mg(+)_{in}$ is only about 5.8×10^{18} cm^{-3} at

TABLE I. Mg site occupancy and lattice parameter obtained by Rietveld refinement and reliability factors of each refinement.

Sample name	Starting composition	Mg site occupancy	Lattice parameter (Å)	R_P	χ^2
$Mg(-)_{in}$	$Mg_{2.24}Si_{0.4}Sn_{0.6}$	1.986 ± 0.008	6.6017 ± 0.0002	8.49	1.45
$Mg(-)_{Sb}$	$Mg_{2.24}(Si_{0.4}Sn_{0.6})_{0.985}Sb_{0.015}$	1.972 ± 0.009	6.6030 ± 0.0003	9.31	1.30
$Mg(+)_{in}$	$Mg_{2.34}Si_{0.4}Sn_{0.6}$	1.998 ± 0.008	6.6023 ± 0.0002	9.08	1.69
$Mg(+)_{Sb}$	$Mg_{2.34}(Si_{0.4}Sn_{0.6})_{0.985}Sb_{0.015}$	2.003 ± 0.009	6.6042 ± 0.0003	8.09	1.29

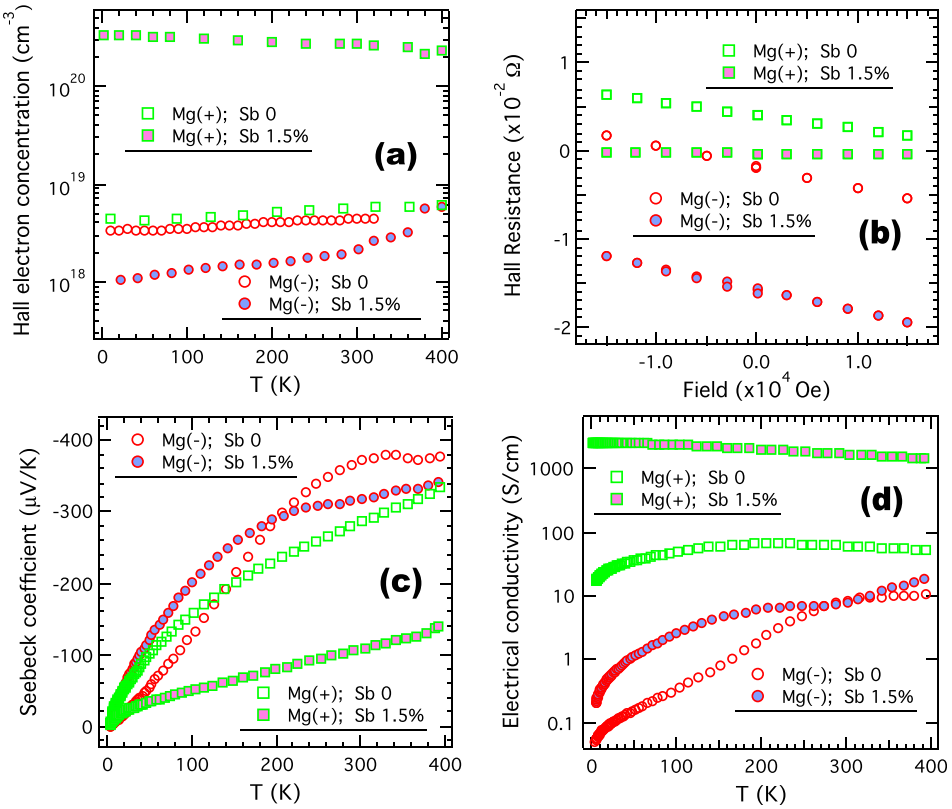

FIG. 2. (a) Temperature-dependent Hall carrier concentration. (b) Plot of Hall resistance (ρ_H) vs. field (H) measured at 300 K. The Hall coefficient is the product of the slope ($d\rho_H/dH$) and the thickness of a sample. The sign of the slope distinguishes electrons or holes as the majority carrier; a negative slope indicates electron conduction; and a positive slope indicates hole conduction. (c) and (d) Temperature-dependent Seebeck coefficient and electrical conductivity of the undoped $Mg_2Si_{0.4}Sn_{0.6}/Mg_{2-\delta}Si_{0.4}Sn_{0.6}$ and Sb-doped samples.

room temperature. Such a low electron density may come from a trace amount of Si or Sn vacancies. With 1.5 mol. % of Sb doping, the n_H of Mg(+) sample increases dramatically to 2.7×10^{20} cm^{-3} at room temperature. It is evident that the Sb dopants in Mg(+)$_{Sb}$ are fully ionized as the extrinsic electron density (2.7×10^{20} cm^{-3}) is approximately equal to the Sb dopant density (2.1×10^{20} cm^{-3}). The Seebeck coefficient (S) and electrical conductivity (σ) of both Mg(+) samples are shown in Figs. 2(c) and 2(d). Mg(+)$_{Sb}$ exhibits a typical degenerate-semiconductor behavior: the absolute value of S rises linearly while σ drops as T increases, which indicates that Sb doping effectively raises the Fermi level into the conduction band. Compared with Mg(+)$_{Sb}$, Mg(+)$_{in}$ exhibits a much higher S and lower σ values, which is consistent with its lower carrier concentration. Moreover, Mg(+)$_{in}$ shows a smooth insulator-to-metal transition with increasing temperature: σ gradually rises as temperature increases but starts to drop above 250 K. The details of this transition are discussed in Section III E.

While the transport properties of the Mg(+) samples are expected and understandable, those of the Mg(–) samples are not. First, Mg(–)$_{in}$ is an n-type semiconductor, as both the Hall coefficient (R_H) and S are negative (shown in Figs. 2(b) and 2(c)). It is known that intrinsic $Mg_2Si_{0.4}Sn_{0.6}$ is a semiconductor and its sign of R_H and S is sensitive to the nature of trace impurities. With a rigid-band model, Mg vacancies contribute two holes to the valence band, which would shift the Fermi level into the valence band and give rise to a p-type R_H and S. Apparently, our experimental results contradict the prediction of a rigid-band model. Second, Sb dopants in the Mg(–) sample do not lead to an increase of the electron concentration. In comparison, the same amount of Sb doping in the Mg(+) sample increased the electron concentration by two orders of magnitude. Fig. 2(a) shows that the electron concentrations at room temperature are 4.3×10^{18} cm^{-3} and 2.1×10^{18} cm^{-3} for Mg(–)$_{in}$ and Mg(–)$_{Sb}$, respectively. The n_H of Mg(–)$_{Sb}$ is even lower than that of Mg(–)$_{in}$. The S and σ shown in Figs. 2(c) and 2(d) indicate that both of the Mg(–) samples behave as semiconductors. To understand these peculiar properties of Mg(–) samples, we formulate a hypothesis that Mg vacancies do not create free holes in the valance band but rather induce localized hole states that trap the electrons provided by Sb doping.

C. DFT electronic structure calculation

The DOS from the PBE level of calculations is consistent with the rigid band model, where Mg vacancies only shift the Fermi level into the valance band and hole states formed are delocalized. However, it is well known that self-interaction errors in pure DFT introduce artificial delocalization and severely underestimate band gaps. The hybrid HSE functional better describes semiconductors, by including a portion of exact exchange. The HSE calculated DOS configurations of $Mg_2Si_{0.375}Sn_{0.625}$ with and without 1.85% Mg vacancies are shown in Fig. 3. Fig. 3(b) shows that the hole state induced by Mg vacancy is separated from the valance band. The inset shows that the state is mainly localized on the four Si/Sn atoms nearest to the Mg vacancy site. As one Sb dopant is introduced to a Si/Sn site, as shown in Fig. 3(c), the hole state is singly occupied by a donor electron from Sb and the DOS splits again as a result of electron-electron interactions associated with the introduction of a second electron. Fig. 3(d) shows that until the concentration of Sb reaches twice that of the Mg vacancies, all the donor

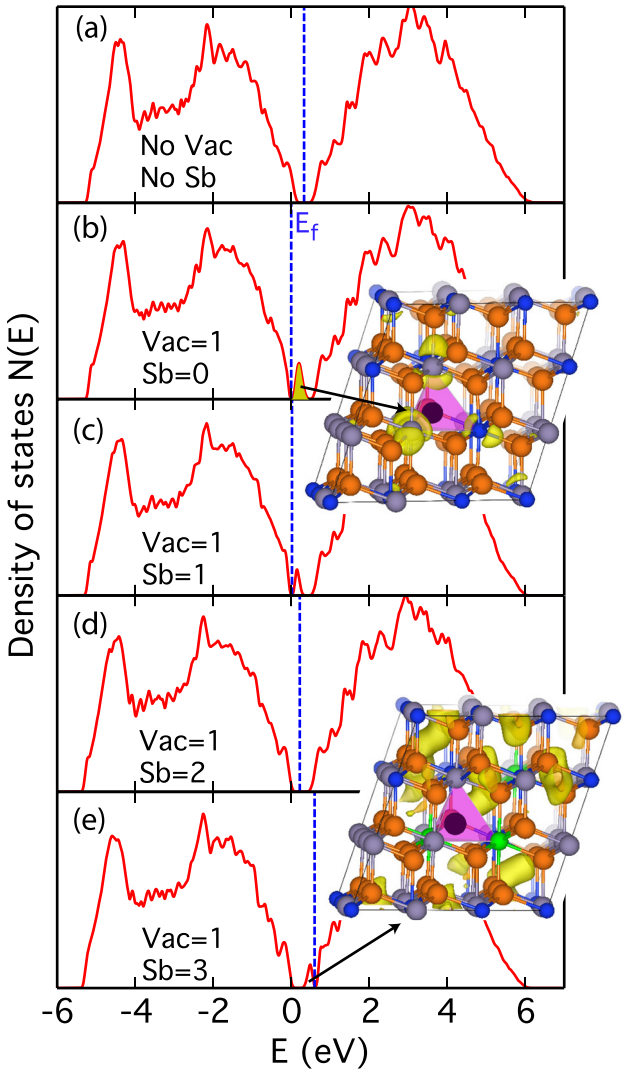

FIG. 3. Density of states for (a) stoichiometric $Mg_2Si_{0.375}Sn_{0.625}$ and (b)–(e) $Mg_2Si_{0.375}Sn_{0.625}$ with one Mg vacancy (1.85%) and a variety of Sb dopants in a $3 \times 3 \times 3$ supercell. The Fermi levels are indicated with blue dashed lines. The energy levels between different Sb concentrations are aligned according to low-energy electronic states. In the insets, the yellow clouds show the electron distribution in real space of the localized state, indicated by black arrows: the hole state is shown in (b) and the donor state in (e). The vacancy site is represented as a black sphere in the magenta tetrahedron. Atoms are colored as: blue for Si; grey for Sn; orange for Mg; and green for Sb.

electrons from Sb are trapped, leaving no conduction band electrons in the material. Therefore, samples with Mg vacancies exhibit poor conductivity even with a moderate amount of Sb doping. A partially occupied localized state may carry magnetic moment. However, our calculation shows that the hybridization between the localized state and the band state is so strong that magnetic moment is screened at any level of doping. At all doping levels, the valance band remains full, which explains why no p-type conduction is observed in this series of materials. When the Sb concentration is high enough, the Fermi level is raised to the bottom of the conduction band, as shown in Fig. 3(e). Although a minimum in the DOS still appears near the Fermi level, the electron distribution of the highest occupied state (in real space) is more extended and not localized around the vacancy or Sb sites. In other words, when the Sb doping density exceeds double of the Mg vacancy density, electrons around Fermi level appear to be itinerant and the material becomes a degenerate semiconductor. This description is consistent with those previous experimental studies that show that $Mg_2Si_{1-x}Sn_x$ behaves metallic when Sb dopant density exceeds twice of Mg vacancy density.[4–6]

D. Localized-electron behavior in $Mg_{2-\delta}Si_{0.4}Sn_{0.6}$

In Section III C, our DFT calculation predicted that in $Mg_{2-\delta}Si_{0.4}Sn_{0.6}$, the Mg-vacancy ($V_{Mg}$) hole states lie in the band gap and the Fermi level lies in between the V_{Mg} states and the valence band. The measured transport properties of $Mg(-)_{in}$ shown in Fig. 2 suggest that there exists a low concentration of electrons (equivalent to 0.03 mol. % one-electron dopants) in the localized states. Our assumption is that these electrons are introduced by a trace amount of Si/Sn vacancies ($V_{Si/Sn}$) resulting from the Sn precipitation during synthesis. The in-gap V_{Mg} states, together with the $V_{Si/Sn}$ electrons, could account for the n-type conductivity observed in $Mg_{2-\delta}Si_{0.4}Sn_{0.6}$. Furthermore, these $V_{Si/Sn}$ can be attracted to Mg vacancies and from ($V_{Si/Sn}V_{Mg}$) complex. This complex would create occupied localized states that are on top of the valence band but below the empty V_{Mg} states. Thermal excitation of electrons from these occupied states to the empty V_{Mg} states would not create p-type conductivity since the holes would be trapped in these ($V_{Si/Sn}V_{Mg}$) localized states.

In addition, the DFT calculations in Section III C also explain the low electron density in $Mg(-)_{Sb}$. As shown in Fig. 3(b), if the V_{Mg} states are partially filled by electrons due to Sb doping, the filled states merge into the valence band. The DOS around the Fermi level is thus reduced, resulting in a slight decrease in electron density in $Mg(-)_{Sb}$.

In this section, we show that this localized V_{Mg} states model is further supported by the localized-electron behaviors manifest in transport properties of Mg(–) samples. Fig. 2(c) shows how the Seebeck coefficient of Mg(–) varies as a function of temperature. Above 350 K, there is a plateau where the Seebeck coefficient value is high, but only weakly temperature-dependent. This behavior is characteristic of localized carriers, whose Seebeck coefficient is described by the Heikes formula, $S = \frac{k_B}{e} ln \frac{1-z}{z}$, where k_B is the Boltzmann constant, e is the electron charge, and z is the ratio of carriers to sites,[15] which is constant when the number of mobile carriers is constant. A similar behavior also shows up in $Mg(-)_{Sb}$, but the plateau moves to a lower temperature, as the activation energy for electron transfer is reduced by the greater occupancy of trap states.

The electrical conductivity depends on two components: the carrier density and carrier mobility. In order to distinguish between these two components, we made a normalized Arrhenius plot of electrical conductivity (σ), Hall mobility (μ), and Hall carrier concentration (n_H) in Fig. 4. For $Mg(-)_{in}$, the temperature-dependence of σ is dominated by μ over the entire measured temperature range. The increase of μ with temperature indicates thermally excited electron hopping between localized states. For $Mg(-)_{Sb}$, the thermally

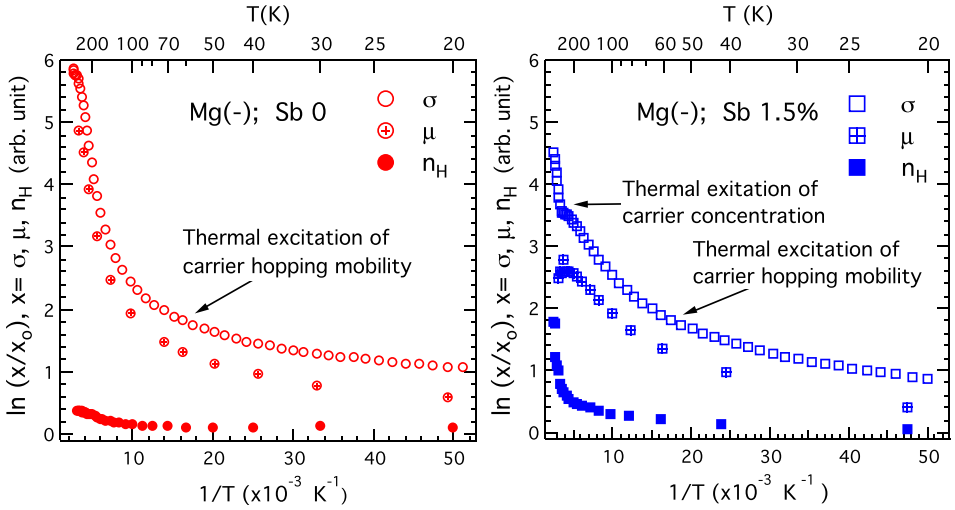

FIG. 4. Normalized Arrhenius plot of electrical conductivity (σ), Hall mobility (μ), and Hall carrier concentration (n_H) for Mg(–)$_{in}$ (left) and Mg(–)$_{Sb}$ (right).

excited electron hopping also dominates the increase of σ vs. T at $T < 300$ K. At $T > 300$ K, n_H increases abruptly, indicating a thermal excitation of carriers. It is possible that Sb doping in Mg(–)$_{Sb}$ raises the Fermi level in the gap states, making it easier to excite electrons.

E. Localized states at conduction band tail

We have previously described Mg-vacancy induced localized states within the band gap. Here, we present evidence for other localized states (the band-tail states) at the bottom of the conduction band edge. As mentioned in Section III B, the electrical conductivity of intrinsic Mg(+) shows a smooth MIT around 250 K. We have also observed similar behaviors in several Sb-doped $Mg_2Si_{0.4}Sn_{0.6}$ materials with a small Mg-deficiency (results not shown in this work). The atomic disorder on Si/Sn site or the Sb impurity dopants create a perturbation of the periodic potential, which create Anderson localized states at a band edge. This MIT from Anderson localization in the band tail is the result of increasing E_F across the mobility edge. Anderson showed that with a large degree of lattice disorder, the diffusion of a one-electron wave function might be absent at 0 K.[16] Mott proposed that a gap can form when the Fermi level is below a mobility edge E_C, which separates localized electronic states from the band states.[17,18] It was noted that if $E_C - E_F > k_BT$, hopping transport dominates; if $E_C - E_F < k_BT$, band transport dominates. When E_F is located in the energies of the localized band-tail states close to E_C, one would observe a transition of electrical conductivity from non-metallic to metallic behavior as temperature increases.

The temperature-dependent electrical conductivity of Mg(+)$_{in}$ can be well interpreted with the mobility-edge model. At 0 K, E_F is located in the energies of the localized band-tail states. As shown in Fig. 5, at lower temperature, the Hall mobility increases with temperature, which indicates that electrons are thermally excited from localized states to band states. In this stage, the temperature-dependence of electrical conductivity can be described by as: $\sigma = \sigma_o \exp[-\frac{(E_C-E_F)/2}{k_BT}]$.[19] With increasing temperature, when $k_BT > E_C - E_F$, the electrical conductivity and charge mobility start to decrease with increasing temperature (shown in Figs. 2(d) and 5), as expected in a degenerate semiconductor due to electron scattering.[20,21]

In contrast, the Fermi level of Mg(+)$_{Sb}$ falls well inside the conduction band and exhibits a metallic conductivity over the entire temperature range. While Mg(–)$_{in}$ has the Fermi level in the localized in-gap V_{Mg} states and thus exhibits a hopping behavior.

IV. CONCLUSIONS

We have presented a localized electron model to account for the intriguing transport properties of the $Mg_{2-\delta}Si_{0.4}Sn_{0.6}$ solid solution with Mg vacancies. We have demonstrated that Mg vacancies, instead of contributing free holes, create localized empty states that trap electrons

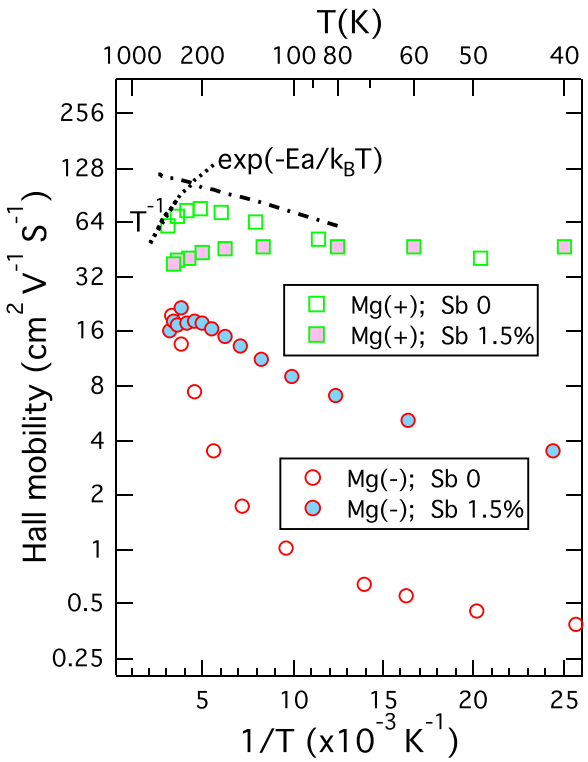

FIG. 5. Temperature-dependent Hall mobility of all samples in this work; the vertical axis is on a natural log scale.

introduced with dopants. The DOS, as calculated with DFT, confirms that Mg vacancies indeed create isolated hole states in band gap. When doped with Sb, the donor electrons are trapped in these localized hole states until the density of Sb dopants exceeds double of that of the Mg vacancies. This localized-electron model is manifest by the localized-electron behavior in the Seebeck coefficient near room temperature as well as the observed thermally activated hopping conductivity. In addition, we have demonstrated a thermally driven insulator-metal transition as the Fermi level, E_F, crosses the mobility edge, E_C, located at the conduction band tail in the lightly electron-doped $Mg_2Si_{0.4}Sn_{0.6}$ material (e.g., $Mg(+)_{in}$).

Mg vacancies in $Mg_{2-\delta}Si_{0.4}Sn_{0.6}$ can be created during synthesis or in subsequent heat treatments when Mg is oxidized or evaporated from the material. Mg vacancies create localized states that neutralize the Sb doping effect. Moreover, the electrical conductivity can be significantly reduced if the Fermi level falls within the localized Mg-vacancy states or the band-tail states with E_F below the mobility edge. The formation of Mg vacancies is a problem, which must be resolved to enhance the performance of the silicides in practical thermoelectric devices. In addition, our results may lead to a new approach to improve the thermoelectric properties by creating resonant states between the localized states and the band states.

ACKNOWLEDGMENTS

This work was supported by National Science Foundation (NSF)-Department of Energy (DOE) Joint Thermoelectric Partnership (NSF Award No. CBET1048767). The SPS equipment used for materials consolidation was acquired with the support of a NSF Major Research Instrumentation (MRI) Award No. DMR-1229131. The PPMS instrument for Hall and electrical transport measurements was acquired with the support of the NSF Materials Interdisciplinary Research Team (MIRT) Award No. (DMR1122603).

[1]V. Zaitsev, M. Fedorov, E. Gurieva, I. Eremin, P. Konstantinov, A. Y. Samunin, and M. Vedernikov, Phys. Rev. B **74**, 045207 (2006).
[2]Q. Zhang, J. He, T. Zhu, S. Zhang, X. Zhao, and T. Tritt, Appl. Phys. Lett. **93**, 102109 (2008).
[3]W. Liu, X. Tan, K. Yin, H. Liu, X. Tang, J. Shi, Q. Zhang, and C. Uher, Phys. Rev. Lett. **108**, 166601 (2012).
[4]G. Nolas, D. Wang, and M. Beekman, Phys. Rev. B **76**, 235204 (2007).
[5]T. Dasgupta, C. Stiewe, R. Hassdorf, A. Zhou, L. Boettcher, and E. Mueller, Phys. Rev. B **83**, 235207 (2011).
[6]G. Jiang, J. He, T. Zhu, C. Fu, X. Liu, L. Hu, and X. Zhao, Adv. Funct. Mater. **24**, 3776 (2014).
[7]J. Tobola, S. Kaprzyk, and H. Scherrer, J. Electron. Mater. **39**, 2064 (2010).
[8]L. Zhang, P. Xiao, L. Shi, G. Henkelman, J. B. Goodenough, and J. Zhou, J. Appl. Phys. **117**, 155103 (2015).
[9]P. E. Blöchl, Phys. Rev. B **50**, 17953 (1994).
[10]G. Kresse and D. Joubert, Phys. Rev. B **59**, 1758 (1999).
[11]J. P. Perdew, K. Burke, and M. Ernzerhof, Phys. Rev. Lett. **77**, 3865 (1996).
[12]J. Heyd, G. E. Scuseria, and M. Ernzerhof, J. Chem. Phys. **118**, 8207 (2003).
[13]J. Heyd and G. E. Scuseria, J. Chem. Phys. **121**, 1187 (2004).
[14]J. Heyd, G. E. Scuseria, and M. Ernzerhof, J. Chem. Phys. **124**, 219906 (2006).
[15]R. R. Heikes and R. W. Ure, *Thermoelectricity: Science and Engineering* (Interscience Publishers, 1961).
[16]P. W. Anderson, Phys. Rev. **109**, 1492 (1958).
[17]N. Mott, Philos. Mag. **13**, 989 (1966).
[18]N. Mott, Adv. Phys. **16**, 49 (1967).
[19]N. F. Mott and E. A. Davis, *Electronic Processes in Non-Crystalline Materials* (Oxford University Press, 2012).
[20]V. I. Fistul and J. Blakemore, Am. J. Phys. **37**, 1291 (1969).
[21]X. Liu, T. Zhu, H. Wang, L. Hu, H. Xie, G. Jiang, G. J. Snyder, and X. Zhao, Adv. Energy Mater. **3**, 1238 (2013).